FEDERAL RESERVE BANK OF SAN FRANCISCO

WORKING PAPER SERIES

Weather, Mobility, and COVID-19: A Panel Local Projections Estimator for Understanding and Forecasting Infectious Disease Spread

Daniel J. Wilson
Federal Reserve Bank of San Francisco

February 2021

Working Paper 2020-23

https://www.frbsf.org/economic-research/publications/working-papers/2020/23/

Suggested citation:

Wilson, Daniel J. 2021. "Weather, Mobility, and COVID-19: A Panel Local Projections Estimator for Understanding and Forecasting Infectious Disease Spread," Federal Reserve Bank of San Francisco Working Paper 2020-23.
https://doi.org/10.24148/wp2020-23

Weather, Mobility, and COVID-19: A Panel Local Projections Estimator for Understanding and Forecasting Infectious Disease Spread*

Daniel J. Wilson†

2/27/21

Abstract

This paper develops an econometric panel data model that can be used both to identify the dynamic effects of disease transmission factors and to forecast disease spread. The empirical model is derived from the canonical SIR epidemiological model of infectious disease spread. The model is estimated using near real-time, county-level data on mobility, weather, and COVID-19 cases. Both mobility and weather are found to have significant effects on COVID-19 effects up to 70 days ahead. Predicted values from the estimated model, augmented to incorporate recent vaccinations, provide out-of-sample forecasts of COVID-19 infections at the county and national levels. Prior forecasts are shown to have been fairly accurate, especially in terms of the geographical/cross-sectional distribution of COVID-19 infections and in terms of the national aggregate forecast. The latest forecasts, using data through February 19, 2021, predict steep declines in infections in most parts of the country over the next several weeks. Nationally, infections are predicted to fall by 59% over the subsequent 30 days. Decomposing the drivers of the latest forecast, the model indicates that accumulated natural immunity (i.e., cumulative infections to date, a.k.a. "seroprevalence") is the primary factor exerting a strong downward pull on new infections.

*I thank Regis Barnichon, Sylvain Leduc, Karel Mertens, Enrico Moretti, Brigitte Roth Tran, Adam Shapiro, Mauricio Ulate, and numerous seminar participants for feedback. I am especially grateful to David Lucca for advice and encouragement on using the SIR model to guide empirics. I also thank Sam Tarasewicz for excellent research assistance and Brad Praiswater for assistance with computing resources. The views expressed in this paper are solely those of the authors and do not necessarily reflect the views of the Federal Reserve Bank of San Francisco, or the Board of Governors of the Federal Reserve System.

†Federal Reserve Bank of San Francisco, daniel.wilson@sf.frb.org

1 Introduction

Understanding and predicting the effects of individual mobility behavior, weather, and other factors on the subsequent spread of infectious diseases like COVID-19 is clearly of first-order public health and economic importance. Public health officials need to know the impact of mobility, which can be mediated by policy actions, on disease spread, especially in severe pandemics like that of COVID-19 when the health consequences can be catastrophic. In addition, individual mobility is integrally linked to economic activity.[1] It is thus important for policymakers to understand the influence of policy-induced economic restrictions and reopenings on disease spread, particularly in pandemics. More generally, it is crucial for policymakers and the public in the midst of a pandemic such as COVID-19 to be able to forecast infections as accurately as possible, accounting for recent changes in mobility and other transmission factors.

This paper develops a semi-structural, econometric panel data model, derived from the standard SIR model of infectious disease spread. The model is used both to identify the dynamic causal effects of transmission factors and accumulated natural immunity as well as to forecast infections out-of-sample. I focus on the transmission factors of mobiity and weather, the importance of which has been suggested by the prior literature.[2] I estimate the model for COVID-19 infections using high-frequency data from over 2,000 counties across the United States, from the start of the pandemic through early December.

I first examine the implied impulse response functions (IRFs) for COVID-19 infections with respect to shocks to weather and mobility. The IRFs run from 10 days ahead to 70 days ahead. To identify plausibly exogenous movements ("shocks") in mobility, I use standard regression control techniques in a dynamic panel data framework. In particular, when

[1]For example, Chen & Spence (2020) document that across countries the drop in GDP in the first quarter of 2020 was highly correlated with declines in mobility. In addition, Barro et al. (2020) show that countries hit hardest by the 1918-19 influenza saw the largest declines in GDP and consumption over 1918 to 1920.

[2]See, e.g., Soucy et al. (2020), Badr et al. (2020), Kapoor et al. (2020), and Glaeser et al. (2020). Most similar to this paper is Unwin et al. (2020), which estimate the impact of mobility on the effective virus reproduction number, R_t, which determines growth in active infections according to the SIR/SIER model. They estimate this impact with state panel data using a logit model with state-specific random effects and inferring the latent $\mathcal{R}_t$ from observed COVID-19 deaths using a Bayesian semi-structural model. The fitted model is used to predict the *current* (i.e., to "nowcast") $\mathcal{R}_t$ and the number of active infections, though it is not used for out-of-sample forecasting. There is also a fairly large number of recent studies on the impacts of non-pharmaceutical interventions, such as shelter-in-place orders. See, e.g., Hsiang et al. (2020) and Flaxman et al. (2020). The prior evidence on weather's impact on COVID-19 is mixed. Xu et al. (2020) finds a "modest" negative effect of temperature on covid19 case growth globally. Carleton et al. (2020) finds a negative relationship between UV light and COVID-19 case growth, while they find "weak or inconsistent lagged effects of local temperature, specific humidity, and precipitation." By contrast, Carson et al. (2020) find strong evidence of a negative temperature effect on COVID-19 transmission in the U.S. based on a state-level panel data model.

regressing future COVID-19 outcomes on current mobility, I control for current growth in COVID-19 infections, current and lagged mobility, weather (temperature and precipitation), county-specific time trends, and high-dimensional fixed effects for counties and for time. Controlling for current and lagged cases and/or deaths, as well as testing, accounts for the likelihood that news of current local COVID-19 spread, which itself would predict future cases and deaths, induces people to increase or decrease their current social distancing (mobility) behavior. Controlling for lagged mobility helps ensure that current movements in mobility are not driven simply by persistence from past mobility shocks. Including county fixed effects effectively controls for many important known and unknown characteristics of local communities that can increase COVID-19 transmission and/or lethality, such as demographics, socioeconomic status, density, etc.

Estimating this model using data from the start of the pandemic through the latest available yields four interesting results. First, changes in mobility behavior have large effects on COVID-19 infections over the subsequent few weeks: current increases (decreases) in mobility increase (decrease) active infections around 20 to (at least) 70 days ahead. Second, changes in temperature also have significant effects, with colder temperatures generally leading to higher growth in COVID-19 infections. Third, holding mobility and weather fixed, COVID-19 growth within a county is generally negatively autocorrelated. That is, local growth in infections tends to be mean-reverting. Fourth, higher cumulative infections to date (accumulated natural immunity, a.k.a., seroprevalence) is associated with lower growth in active infections, consistent with the SIR model.

Predicted values from the model using the latest available data, augmented to account for recent vaccinations, provide forecasts of COVID-19 infections by county for horizons from 10 days to 70 days ahead. The latest forecasts point to steep declines in active COVID-19 infections in Southern California, Arizona, Texas, and much of the south, while infections are predicted to rise in the upper midwest and some parts of the northeast. Aggregating to the national level, these forecasts indicate that active infections are predicted to continue falling steeply over the next few weeks. In particular, the forecast predicts a change in log points of -0.90, which is equivalent to a percentage change of -59%, for the 30-day ahead horizon.

Assessing the accuracy of prior forecasts – i.e., quasi-out-of-sample forecasts based on data and model estimation available at prior points in time – suggests a fairly high degree of accuracy, especially at horizons of up to about 40 days. In particular, forecast accuracy tests point to three findings. First, the cross-county correlation between forecasted growth and actual growth are generally high, ranging from .44 to .68 in the most recent past forecasts, and they tend to increase with the forecast horizon. This suggests the forecasting model is

useful for predicting which parts of the country are most likely to experience strong increases (hot spots) or decreases in the weeks ahead. Second, at the national level, the difference between forecast growth (column 4) and actual growth (column 3) is quite small for the first few horizons but grows large for the farthest out horizons (60 days and beyond). For instance, the 30-day ahead forecast of the change in log active infections using data as of January 10, 2021 was -0.99 (equivalent to -63%), which is very close to the actual change in log active infections for that period of -0.98 (-62%). Third, despite the strong accuracy at the national level, the typical forecast error at the county level, as measured by the root mean-squared forecast error (RMSFE), is large and increases with the forecast horizon, suggesting that the forecasts for any given county should be treated with caution.

In the final part of the paper, I use the forecasting model to examine what factors are driving the recent and projected steep declines in COVID-19 infections. The results indicate that accumulated natural immunity was the dominate driver of the declines in infections since early January and will remain the dominate driver of declines over at least the next 30 days. The model suggests that reduced mobility played a modest role in the decline in infections from early January to date, while weather (in particular, cold winter temperature) prevented an ever faster decline. The model shows no meaningful role yet for vaccinations because, as of mid-February, they covered only a small share of the population.

This paper also builds and improves upon earlier efforts at forecasting COVID-19 outcomes, especially at the subnational level. Liu et al. (2021) estimates "a dynamic panel data model to generate density forecasts for daily active Covid-19 infections for a panel of countries/regions." The model assumes that the growth rate of infectious individuals in each country/region follows a downward-sloping deterministic time trend. Such models can be quite useful in data-scarce settings and early in pandemics when the key factors driving transmission are either unknown or not observed in data. By contrast, the present paper exploits rich panel data on mobility and weather to generate forecasts of infections reflecting not only recent infections but also these observed transmission factors.

The data-driven, econometric forecasting approach developed in this paper contrasts with, and complements, the more structural epidemiological modeling approach used by many other forecasters. The econometric approach relies on far fewer assumptions about virus characteristics and social distancing behavior. Rather, it assumes the historical relationships between transmission factors and COVID-19 spread, and the dynamics of COVID-19 spread, over the course of the pandemic to date will continue to hold over the forecast horizon.[3] It is also important to distinguish this approach – which provides *forecasts* of fu-

[3]Many such projection models are used by the CDC in formulating their ensemble forecast. See `https://www.cdc.gov/coronavirus/2019-ncov/cases-updates/forecasts-cases.html`.

ture COVID-19 infections based on data as close to real-time as possible – from approaches, such as Fernández-Villaverde & Jones (2020), Lemaitre et al. (2020), and others that provide *scenario projections* under various alternative scenarios regarding behavior factors such as mobility. Those projection models also generally are not estimated using panel data methods, which naturally account for unobserved local characteristics (e.g., county fixed effects), and very few account directly for weather.

2 Data and Stylized Facts

2.1 COVID-19 and Mobility Data

Daily county-level data on COVID-19 cases and deaths were obtained from usafacts.org, which compiled the data from state public health agencies.[4]

I use several alternative measures of individual mobility behavior. The first is the Dallas Federal Reserve Bank's Mobility and Engagement Index (MEI), which is the first principal component of seven device geolocation variables obtained the data provider Safegraph, and is a composite measure of time spent and distance away from home.[5]

I also use measures of mobility from the Google Mobility Reports. These data measure percent changes in mobility relative to its Jan. 3 – Feb. 6 average. More specifically, Google describes the data as follows: "These datasets show how visits and length of stay at different places change compared to a baseline. We calculate these changes using the same kind of aggregated and anonymized data used to show popular times for places in Google Maps. Changes for each day are compared to a baseline value for that day of the week: The baseline is the median value, for the corresponding day of the week, during the 5-week period Jan. 3 – Feb. 6, 2020."[6] Google measures mobility separately for visits to workplaces, transit stations, grocery & pharmacy, parks, and retail & restaurants (which includes restaurants, cafes, shopping centers, theme parks, museums, libraries, and movie theaters).

Figure 1 shows how two broad mobility measures have evolved since late January nation-

[4] `https://usafactsstatic.blob.core.windows.net/public/data/covid-19/covid_confirmed_usafacts.csv`

[5] The seven variables are as follows: the fraction of devices leaving home in a day, the fraction of devices away from home for 3-6 hours at a fixed location, the fraction of devices away from home longer than 6 hours at a fixed location, an adjusted average of daytime hours spent at home, the fraction of devices taking trips longer than 16 kilometers, the fraction of devices taking trips less than 2 kilometers, and the average time spent at locations far from home. Each variable is scaled by the weekday-specific average over January and February prior to the principal component analysis. See Atkinson et al. (2020) for details. The data were accessed at `https://www.dallasfed.org/~/media/documents/research/mei/MEI_counties_scaled.csv`.

[6] The data were accessed at `https://www.google.com/covid19/mobility/`.

ally as well as in some selected cities. For the nation as a whole, overall mobility plunged over the second half of March 2020, bottomed out in early April, and partially recovered through late June. Mobility remained relatively stable until early autumn, at which time it began to fall again. It has risen somewhat again in early February. Yet, there was considerable variation across places. Some places, such as San Francisco (County) and New York City, saw mobility fall much sooner and further than it did nationally. In other places, such as Miami and Phoenix, mobility fell around the same time as it did nationally but by a smaller amount. The recovery pattern also varied substantially across places. For example, mobility recovered relatively quickly from April to July in New York City, while mobility recovered more slowly and modestly over that period in San Francisco. It is this type of variation – that is, the variation across counties in their differences from the national average – that I exploit to estimate the impact of mobility on subsequent COVID-19 outcomes.

2.2 Weather Data

Following Wilson (2019), I construct measures of daily weather at the county level from the Global Historical Climatology Network Daily (GHCN-Daily) data set. The GHCN-Daily is provided by the U.S. National Climatic Data Center (part of the National Oceanic and Atmospheric Administration (NOAA)) and contains daily weather measurements from a little over 4,700 weather stations throughout the United States, though not all stations provide readings every day. All stations with data on a given date are used for measuring county weather on that date. The spatial distribution of weather stations is highly correlated with the spatial distribution of population.

The readings from individual weather stations are used to estimate county-level weather using an inverse-distance weighting procedure. First, the surface of the conterminous United States is divided into a 5-mile by 5-mile grid. Second, weather values for each grid point are estimated using inverse-distance-weighted averages of the weather values from weather stations within 50 miles of the grid point. See Wilson (2019) for further details of this procedure. This procedure yields the daily county-level measures of maximum temperature (degrees Fahrenheit) and precipitation (mm).[7]

[7]I also obtained measures of snowfall, though I do not include it in the analyses shown in this paper because there is very little variation in snowfall during the sample period used in the analyses, which is generally late spring through early winter. Including snowfall as an additional weather variable in the regressions below has virtually no impact on the results.

3 Methodology

In this section, I derive an empirical model guided by the canonical epidemiological model of infectious disease spread that can be used both to identify the dynamic causal effects of transmission factors as well as to forecast disease spread. The epidemiological model provides a basic characterization of the process by which infections evolve over time as a function of transmission factors such as individual mobility behavior and weather.[8] This process motivates an empirical dynamic panel data model that can be used to estimate infection impulse response functions (IRFs) with respect to shocks to mobility, weather, or other factors. As shown in Section 5, the empirical model can also be used to provide out-of-sample forecasts of infections.

3.1 Infectious Disease Spread According to the Standard SIR Model

The canonical epidemiological model of infectious disease spread is known as the Susceptible-Infected-Removed (SIR) model. In the standard SIR model (see, for example, Anderson, et al. (1992)), the number of infectious individuals in a population evolves according to the following process:

$$I_{t+1} = I_t \left(1 - \gamma + \beta_t s_t\right) \tag{1}$$

where $s_t \equiv \frac{S_t}{N}$ is the susceptible (not previously infected) share of the population (N) as of the end of period t and γ is the rate at which infectious individuals recover or die within period t. The variable, β_t, is the current transmission rate of the virus – that is, the rate at which susceptible individuals, during the interval t, are exposed to and contract the virus from infectious individuals. Note that the term $\beta_t s_t$ is known as the effective reproduction number: $\mathcal{R}_t \equiv \beta_t s_t$.

Let us define the frequency of t as the duration of the infectious period for the virus, for which case $\gamma = 1$. Equation 1 then implies the following evolution of infections from time t

[8] See Bisin & Moro (2020) for a discussion of the empirical implications of standard SIR model as well as of a more general spatial-SIR model.

to h periods ahead:

$$\begin{aligned} I_{t+1} &= I_t \beta_t s_t \\ I_{t+2} &= I_{t+1} \beta_{t+1} s_{t+1} = I_t \left(\beta_t s_t\right) \left(\beta_{t+1} s_{t+1}\right) \\ &\dots \\ I_{t+h} &= I_t \prod_{\tau=0}^{h-1} \beta_{t+\tau} s_{t+\tau}. \end{aligned} \tag{2}$$

Dividing both sides by I_t and taking logs yields:

$$log I_{t+h} - log I_t = log \prod_{\tau=0}^{h-1} \beta_{t+\tau} + \sum_{\tau=0}^{h-1} \left[log \left(s_{t+\tau}\right)\right] \ . \tag{3}$$

In the standard SIR model, without vaccinations, $s_{t+\tau} \equiv 1 - c_{t+\tau}$, where $c_{t+\tau} = \frac{\sum_{j=0}^{t+\tau} I_j}{N}$ (i.e., the share of the population infected to date). Note that $c_{t+\tau}$ is readily observable via data on cases per capita. It is straightforward to expand this model to account for vaccinations. As a greater share of the population not previously infected become effectively vaccinated, these individuals become "removed" from the susceptible population, S_t. In this case,

$$s_{t+\tau} \equiv 1 - c_{t+\tau} - \sigma v_{t+\tau} \left(1 - c_{t+\tau}\right), \tag{4}$$

where $v_{t+\tau} \equiv \frac{\sum_{j=0}^{t+\tau} V_j}{N}$ equals the vaccinated share of the population and σ denotes the vaccine efficacy rate. The above equation assumes that vaccinations, v, are given to both individuals previously infected and not previously infected – consistent with current policy in the U.S.

Given that vaccinations (v), unlike infections (c), have been zero throughout the entirety of our regression sample period until very recently, we separate these two components of $log \left(s_{t+\tau}\right)$ in order to allow each to have different coefficients in the forecasting equation. Specifically, note that:

$$log \left(s_{t+\tau}\right) = log \left(1 - c_{t+\tau}\right) + log \left(1 - \sigma v_{t+\tau}\right). \tag{5}$$

Substituting this expression into equation (2), we get:

$$log I_{t+h} - log I_t = log \prod_{\tau=0}^{h-1} \beta_{t+\tau} + \sum_{\tau=0}^{h-1} \left[log \left(1 - c_{t+\tau}\right)\right] + \sum_{\tau=0}^{h-1} \left[log \left(1 - \sigma v_{t+\tau}\right)\right] \ . \tag{6}$$

Note that $v_t = 0$ until very recently and hence we omit the right-most term for the purposes

of the regression/empirical model derived below.

3.2 Deriving an Empirical Model of Infectious Disease Spread

The key challenge in bringing the above structural model to the data is that first term on the right-hand side of equation 6 – i.e., the product of transmission rates from t to $t+h-1$ – is unobserved. Let us denote that product as β_t^h. I hypothesize that β_t^h is a dynamic function of current and past values of mobility (M) and weather (W)(e.g., temperature).[9] Letting ψ^h and δ^h represent the elasticities of the transmission rate with respect to mobility and weather, respectively, this hypothesis implies the following equation:

$$logI_{t+h} - logI_t = \psi^h m_t + \delta^h w_t + \theta c_{t+h-1}, \tag{7}$$

where $m \equiv log(M)$ and $w \equiv log(W)$.

The specification given by equation 7 is similar in form to the local projections (LP) estimator (Jordà (2005)), which is a common econometric method for estimating impulse response functions (IRFs). The LP estimator, as an alternative to vector auto-regressions (VARs), is far more amenable to panel data settings and is straightforward to implement. As is standard in LP applications, and discussed more in the following subsection, I add lags of the treatment variables of interest, which here are mobility and weather, and a lag of the dependent variable. Adding those terms along with an error term yields the following general regression specification:

$$logI_{t+h} - logI_t = \rho^h dlogI_{i,t} + \sum_{\tau=0}^{P} \psi^{h\tau} m_{t-\tau} + \sum_{\tau=0}^{P} w_t^{'} \delta^{h\tau} + \theta c_{t+h-1} + \epsilon_{t,t+h}, \tag{8}$$

Next, in order to exploit the availability of cross-sectional data at the level of U.S. counties, I add county fixed effects. Lastly, anticipating the use of the model for out-of-sample forecasting of infections h periods ahead given data up to t, I replace $\sum_{\tau=0}^{h-1} log\,(1-c_{t+\tau})$, which captures the accumulated natural immunity of previously infected individuals, from t to $t+h-1$ with $\sum_{\tau=0}^{h-1} log\,(1-c_{i,t+\tau}) = \sum_{\tau=0}^{h-1} log\,(1-c_{it}) = h\ log\,(1-c_{it})$. This simply assumes that the previously infected share of the population is roughly constant over the forecast horizon. This assumption implies the parameter θ^h will partly reflect the degree of autocorrelation of cases per capita. It will also capture any factor of proportionality between known cases and actual cases due to inadequate testing (which is another reason to treat

[9] One could include other potential factors here as well, such as mask-wearing and non-pharmaceutical interventions (NPIs), if they are observable in the data. I consider those two particular factors in additional analyses provided in Section 4.

cases and vaccinations separately). With these additions, the final baseline specification becomes:

$$logI_{i,t+h} - logI_{it} = \rho^h dlogI_{i,t} + \sum_{\tau=0}^{P} \psi^{h\tau} m_{i,t-\tau} + \sum_{\tau=0}^{P} w_{it}^{'} \delta^{h\tau} + \theta c_t + \alpha_t^h + \alpha_i^h + \epsilon_{i,t,t+h}, \quad (9)$$

where $dlogI_{i,t} \equiv logI_{it} - logI_{i,t-1}$ and i indexes counties.

The local projections method traces out an impulse response function (IRF) by estimating equation 9 sequentially over horizons from $h = 1$ to some maximum horizon, H. The IRF for mobility is traced out by the sequence of $\psi^{h,0}$, while the IRF for any measure of weather w_{it} is traced out by the sequence of its coefficient $\delta^{h,0}$. Note that the log-log form of the specification implies that $\psi^{h,0}$ and $\delta^{h,0}$ can be interpreted as elasticities.

Up to this point, the frequency of the time dimension for this empirical model has been unspecified. As noted above, the length of time represented by the period t should correspond to the length of time in which an individual is infectious. For COVID-19, while the actual infectious period varies by individual and situation, the latest summary of research by the Centers for Disease Control and Prevention concludes that in the vast majority of cases the infectious period is below 10 days and may even be below 6 days.[10] However, there is also be a few-days incubation period between exposure and infectiousness. Taking these considerations into account, I assume an infectious period of 10 days.[11] In addition, there is a "confirmation" lag between actual infection and confirmation of a positive test result. The CDC reports that this lag is typically 4 to 5 days. Thus, I measure daily new infections (prior to time-aggregating to the frequency of infectious periods) using confirmed cases 4 days prior. In other words, the number of infectious persons in the 10-day period t (I_t) is proxied by the 10-day sum of confirmed cases as of 4 days prior to the beginning of t. The 10-day period length also has the advantage that day-of-week factors in cases or deaths will get averaged out.

A potential concern with using confirmed cases to measure I_t is that many COVID-19 infections, especially early on in the pandemic, were likely undetected due to incomplete testing. An alternative approach to measuring I_t using deaths data is as follows. If one assumes that deaths occur, on average, k days after infection, then infections on any given day can be proxied by deaths k days ahead. I_t is then simply the 10-day sum of the implied daily infections for the 10-days corresponding to period t. I use this approach in Section 4

[10] `https://www.cdc.gov/coronavirus/2019-ncov/hcp/duration-isolation.html`

[11] To assess robustness, I also estimated the core results of the paper assuming a 7-day infectious period and obtained very similar results.

as a check on the robustness of the main analyses, which relies on the cases data. For that analysis, I assume k equals 21 days following prior studies.

3.3 Incorporating Vaccinations

As shown in equation 6, the SIR model with vaccinations yields an additional term on the right-hand side of the regression specification (equation 9) with a coefficient of 1:

$$\sum_{\tau=0}^{h-1} \left[log\left(1 - \sigma v_{i,t+\tau}\right) \right] \tag{10}$$

where, again, $v_{i,t+\tau}$ equals the vaccinated share of the population and σ denotes the vaccine efficacy rate. I set σ equal to 0.95 based on clinical trial data for two vaccines currently approved in the U.S. To incorporate this component into the forecast model in Section 5, I set $v_{i,t+\tau} = v_{i,t}$, which simplifies the above term to $h \cdot log\left(1 - \sigma v_{it}\right)$, and following equation (6) add it to the predicted values of $logI_{i,t+h} - logI_{it}$.

3.4 Identification

While causal identification is not necessary for forecasting (for which only predictive power is required), it is an important for interpreting the results of the estimated model. As mentioned earlier, the causal effect of mobility, $\beta^{h,0}$, or weather, δ^h, on COVID-19 cases and deaths is unlikely to be identified by any simple cross-sectional correlations due to a variety of omitted variable and reverse causality concerns.[12] The empirical model above addresses these identification concerns through dynamics, control variables, and fixed effects. In terms of dynamics, equation 9 uses leads of the COVID-19 infections as dependent variables to mitigate the potential contemporaneous reverse causality due to local news about current infections inducing people to increase or decrease their social distancing (mobility) behavior. For the same reason, I include the contemporaneous value of the dependent variable (i.e, $dlogI_{it}$). Including the contemporaneous growth in infections ensures that the identifying variation in mobility should not reflect any response of individual mobility to current growth in infections. I additionally include three weekly lags of mobility – i.e., setting $P = 3$ above – so that $\beta^{h,0}$ can be interpreted as the effect of a current "shock" or change in mobility that was not driven simply by autocorrelation driven by an earlier mobility shock.

As the results below will demonstrate, when studying the effect of mobility on COVID-19, it is important to control for weather. Likewise, when studying the effect of weather on COVID-19, it is important to control for mobility. As discussed in the introduction, most

[12] See Goodman-Bacon & Marcus (2020) for a thorough discussion of these concerns.

COVID-19 studies to date of either weather or mobility have not controlled for the other factor and could be subject to serious omitted variable bias. Thus, I include both mobility and weather variables – specifically, maximum daily temperature and precipitation – in all regressions unless otherwise indicated.

The county fixed effects absorb many important known and unknown characteristics of local communities that can increase COVID-19 transmission and/or lethality. These time-invariant characteristics include demographics (such as age, gender, and race), socioeconomic status, access to healthcare, population density, average household size, the presence of nursing homes or meat-packing plants, and openness to international travelers. Desmet & Wacziarg (2020) document the importance of many such time-invariant factors for COVID-19 cases and deaths among U.S. counties. The time fixed effects will absorb seasonal factors (that are not already captured by weather) and any common (i.e., national) time trends.

3.5 Inference

The standard errors and confidence intervals reported in the paper are robust to heteroskedasticity and two-way clustering by county and by time (where time is the 7-day infectious periods). The clustering by county allows for the possibility that the errors, $\epsilon_{i,t,t+h}$, in equation 9, are serially correlated. The clustering by time allows for the possibility that errors are contemporaneously correlated across counties. This clustering will account for cross-county correlation stemming from unobserved state or national factors such as economic and public health policies. It will also account for any geo-spatial correlation in measurement error, for example in weather data.

3.6 Data Sample

All regressions in the paper use the maximum data sample available for the variables used in that regression, though I restrict the sample time period for each county to begin with the first date on which cases per capita exceeded one per 1,000 persons. This restrictions exclude observations from time and places where COVID-19 had not yet begun to spread. The sample time period varies across the local projections regressions depending on the horizon (h) – the further out the horizon, the fewer time periods (t) available for estimation – and on the data availability of the mobility variable used.

Data availability varies across the mobility variables. The Google Mobility data are available from mid-February 2020 through mid-February 2021 as of the time of this writing. None of the mobility variables is available for all counties due to suppression of data (by Safegraph and Google) for counties with fewer mobile devices to mitigate privacy concerns.

The county coverage varies across the mobility measures from just under 1,000 for visits to parks to over 2,800 for the MEI. (There are 3,140 counties in the U.S.)

4 Results from the Estimated Model

4.1 Dynamic Impacts of Mobility on COVID-19

This section describes the results from jointly estimating the impulse response functions (IRFs) of mobility and weather on COVID-19 cases and deaths using the local projections estimator described above (equation 9). As mentioned earlier, the data are measured (averaged) for 10-day intervals. The dependent variables are log new infections at time $t + h$ minus log new infections at time t, for $h = 1$ to 7 periods.

I begin by discussing the estimated IRFs with respect to mobility, which are shown in Figure 2. These IRFs are the sequence of $\psi^{h,0}$ from estimating equation 9 by OLS for each horizon from $h = 1$ to 7 periods ahead. The IRFs are estimated separately for each of the alternative measures of mobility. As derived in Section 3, mobility is measured in log units. For the Google mobility measures, because the raw data are provided in units representing percent changes from a pre-COVID baseline, I first convert the data to index values equal to 1 in the pre-COVID period (by dividing the raw data by 100 and adding 1) prior to taking logs.

Recall that active infections, I, can be measured from data on either confirmed cases or deaths. Given the rarity of deaths relative to cases, I treat the measure based on cases as the preferred, baseline, while presenting results based on deaths as a robustness check. The results based on cases are plotted in Figure 2. Overall mobility is found to have a large positive effect on subsequent growth in COVID-19 infections. Based on the MEI, mobility has a positive and significant effect on infections starting one period (10 days) ahead and it persists through at least 70 days ahead. The peak effect is approximately 60 days ahead. The effects are quantitatively large. The peak coefficient is about 0.9, which implies that a 10 percent increase in mobility results in an approximately 9 percent increase in active infections 60 days ahead.

The IRFs are qualitatively similar for other measures of mobility. For instance, mobility measured by visits to workplaces also peaks around 60 days ahead, though with a larger elasticity around 2.8. Positive and significant effects on infections through the 70-day horizon are also found for visits to transit stations, retail & restaurants, grocery & pharmacy establishments, and parks. These IRFs are also broadly similar if one measures infections based on deaths data instead of cases data (as described in Section 3). Those results are

shown in Figure A1. In general, the IRFs are similar to those in Figure 2 but less precisely estimated.

In sum, mobility is found to have a large positive and long-lasting effect on subsequent growth in COVID-19 infections. The effects appear within 10 days of the mobility shock and persist much later than suggested by prior studies of mobility or governmental social distancing policies (discussed in the introduction), though those studies generally did not investigate effects beyond one month ahead. The long-lasting effects found here can be explained by a propagation mechanism by which mobility increases today result in new infections over the 10 days or so, which result in further new infections with their own incubation periods, which result in further new infections and so on until. This spread can continue indefinitely until herd immunity is reached or can fade to zero if either interpersonal contacts (i.e., mobility) sufficiently falls or medical treatments sufficiently reduce individuals' infectiousness. In fact, it appears that mobility shocks themselves exhibit some persistence but are not permanent. One can obtain the IRF of mobility itself to shock in mobility by simply changing the dependent variable in the LP estimator (equation 9) to log mobility for each horizon h, $m_{i,t+h}$. The results indicate that mobility is positively autocorrelated but with less than a unit root. Mobility shocks tend to die out after 3 to 4 periods (30 to 40 days). (See Online Appendix Figure A2.)

4.2 Dynamic Impacts of Weather on COVID-19

The IRF results for weather are presented in Figure 3. The point estimates are shown with the circles, while the shaded regions indicate the 68 (one standard error), 90, and 95 percent confidence bands (from darkest to lightest). The regressions underlying Figure 3 control for mobility, measured by the MEI. The weather variables here are the log of maximum daily temperature and the level of precipitation (in mm).[13]

Temperature is found to have a large but temporary negative effect on COVID-19 case growth. Specifically, higher temperatures reduce case growth significantly starting as soon as 10 days ahead and for up to 20 to 30 days ahead. The peak coefficient on log temperature occurs around 20 days ahead at approximately -1. This coefficient implies that 10% higher daily maximum temperature during the current time period lowers growth in new COVID-19 infections around one month later by about 10 percent. The temperature effect turns positive at the maximum horizon, 70 days ahead. This positive result, which vanishes when time

[13]I do not take logs of precipitation because of the frequent zero values. Also, as noted in Section 2, I omit snowfall from the model because it is zero for the majority of the sample (which, unlike the sample in the prior subsection, generally covers the warmer months from late spring to late fall because COVID-19 cases were near-zero in most counties until late spring). Snowfall is generally statistically insignificant and including it has very little effect on any of the other results.

fixed effects are dropped as in the model used for forecasting, may reflect that higher (lower) temperatures today reduce infections in the near term but also decrease (increase) aspects of social distancing not captured by the mobility data. Lastly, no statistically significant effect of precipitation is found on growth in infections at any horizon.

The full regression results underlying the weather and mobility IRFs are provided, for a single selected horizon of 30 days ahead and for infections based on cases data, in Table 1. Beyond the results already discussed, the results also show that infections growth is negatively autocorrelated. That is, infections growth tends to be mean-reverting. The table also shows that, consistent with predictions of the SIR model, cumulative cases per capita up to period t, which should be proportional to cumulative infections per capita up to period t, exerts a negative effect on subsequent growth in new infections.

Lastly, it is interesting to consider the adjusted-R^2's, shown at the bottom of Table 1. The regressors in the model, including the county and time fixed effects, explain as much as 52% of the variation in infections growth 30 days ahead.

5 Applying the Model to Forecasting

5.1 Adapting Model for Forecasting

The panel local projections empirical model developed in Section 3.2 is easily adaptable, and highly useful, for providing out-of-sample forecasts at the panel-unit level. Here, I apply this model to provide h-period ahead forecasts of COVID-19 active infections for each county in the U.S. ($I_{i,t+h}$), excluding counties with missing mobility data. For this exercise, I use the Mobility & Engagement Index (MEI) measure of mobility because it has fewer missing counties than the Google Mobility data.

The one element of the baseline local projections estimator in Section 3.2, i.e., equation 9, that is unknown and unestimable as of time t (other than the error term of course) is the h-period ahead time fixed effect, α_t^h. Hence, this term must be omitted to obtain an estimable panel local projections model useful for out-of-sample forecasts. Before using it for forecasting, I first check whether this restricted model behaves similarly in-sample to the baseline model that includes the time fixed effects. The resulting IRFs are quite similar to those of the baseline model (see Online Appendix Figure A3). The in-sample fit of the model suffers modestly by omitting the time fixed effects. One can see this by comparing the adjusted R^2's for the time fixed effects regressions in Table 1 to the corresponding regressions without time fixed effects (provided in Online Appendix Table A1). For example, when mobility is measured by the MEI, the adjusted R^2 drops from 0.46 to 0.35 when time fixed

effects are omitted.

Predicted values from estimating equation (9), modified to omit time fixed effects, using data up to period t, provide provisional forecasts of COVID-19 infections by county for each horizon h. We obtain final forecasts by augmenting these provisional forecasts to account for vaccinations (v_{it}), as described in 3.3. We measure v_{it} using state-level data from Centers for Disease Control and Prevention (CDC) on the share of the population that are fully vaccinated (i.e., received both doses for two-dose vaccines). Counties are assumed to have the same share of their population fully vaccinated as their state's average.

5.2 Local and National Forecasts

Figure 4 visualizes the 30-day ahead forecasts of growth in COVID-19 active infections by county, as of February 19, 2021. That is, the forecasts are the empirical model's predicted values for $logI_{i,t+3} - logI_{it}$, where t corresponds to 10-day intervals (and i denotes a county) using data up to February 19. The forecasts point to steep declines in COVID-19 infections in Southern California, Arizona, Texas, and much of the south. Yet, the model predicts infections are predicted to rise in the upper midwest, likely due to influence of the extreme cold temperatures that occurred there during the days leading up to this forecast.

These county-level forecasts can be aggregated via population-weighted means to provide a national forecast for each horizon. The resulting forecasts for the change in national log active infections for the different horizons can be applied to the latest level of national infections to obtain a forecast for active infections over the next 70 days. The latest national forecast, along with the historical data to date, is plotted in Figure 5. Active infections are predicted to continue falling steeply over the next few weeks. For instance, the forecast predicts a change in log points of -0.90, which is equivalent to a percentage change of -59%, for the 30-day ahead horizon.

5.3 Accuracy of Prior Forecasts

To assess the accuracy of our forecasts, we compare the most recent past forecast, for each horizon, to actual infection growth over the same period. We do this at the county level as well as at the aggregate level (via population-weighted means).

The results are shown in Table 2. For example, the first row evaluates the accuracy of a 10-day ahead forecast of infection growth (i.e., change in log active infections), based on data up until 10 days from the last day of available data, by comparing it to actual growth in infections over those 10 days. The table reveals three general patterns. First, the cross-county correlation (column 1) between forecasted growth and actual growth are fairly high,

ranging from .44 to .68, and they tend to increase with the forecast horizon. This suggests the forecasting model is useful for predicting which parts of the country are most likely to experience strong increases (hot spots) or decreases in the weeks ahead.[14] Second, at the national level, the difference between forecast growth (column 4) and actual growth (column 3) is quite small for the first few horizons but grows large for the farthest out horizons. The 30-day ahead forecast of the change in log active infections is -0.99 (equivalent to -63%), which is very close to the actual change in log active infections for that period of -0.98 (-62%).[15] That said, the typical forecast error at the county level, as measured by the root mean-squared forecast error (RMSFE), is large and increases with the forecast horizon. For instance, the RMSFE for the most recent (past) 30 day ahead forecast is 0.45.

Additional evidence of the performance of the national forecast is provided in Figure 6. The solid black line plots actual data on active/new COVID-19 infections to date. The dashed blue line plots the out-of-sample forecast based on the latest available data. The other series show previous forecasts based on data (and the model estimated with that data) available at the start of each forecast period (indicated by the first dot of each plotted series).[16] The forecasts have tended to be fairly accurate and have improved over time. Notably, the forecast based on data as of Nov. 17, 2020 (the second red series), when infections were increasing rapidly, predicted a continued rapid climb for subsequent 40 days before hitting a peak and starting to decline. This forecast proved generally accurate except that that actual peak occurred about 10 days later than the forecast predicted.

5.4 Key Drivers of Forecasted Declines

The latest national forecast predicts a steep decline in active COVID-19 infections over the next several weeks. In order to assess what factor(s) are driving this decline, one can alternately "turn off" each factor's contribution to the forecast.

We first turn off vaccinations by simply setting $v_{it} = 0$ in equation (2) above. The result is shown by the red dashed line in Figure 7a. The forecast without vaccinations is very similar to the baseline forecast, indicating that vaccinations are NOT a primary driver of the forecasted decline. We next alternately turn off each of the key components from the estimated model (equation (1)).[17]

[14] See Online Appendix Figures A5 and A6 for a visual comparison of the county level forecasts to actual growth for the 30-day ahead horizon.

[15] Log point changes, x, can be converted to percentage changes as follows: $(e^x - 1) \cdot 100$.

[16] The estimated coefficients of the model have been fairly stable over time, indicating that the changes in forecasts over time are driven by changes in the regressors rather than changes in their coefficients.

[17] For any given regressor in the model, this can be done by taking the estimated model from equation (1) and then, instead of plugging in the actual data for that regressor, plugging in its its county-specific means.

The results point to three interesing implications of the forecasting model. First, removing the temperature effect yields a faster predicted decline – that is, colder winter temperatures prevented a faster decline. Second, removing the mobility effect yields a slightly slower predicted decline – that is, declines in mobility in the weeks leading up to the infections peak contributed modestly to the rapid forecasted decline in infections. Third, and most importantly, removing the accumulated natural immunity term, which accounts for each county's population share already infected, yields a strong predicted *increase* in infections over the subsequent 30 days followed by a sharp predicted decline. The initial increase suggests that infections would have continued to surge well into February 2021 if not for the strong downward pull exerted by accumulated natural immunity. Yet, even without this effect, the forecast still predicted an eventual decline due to mean-reversion (i.e., the estimated negative autocorrelation in infection growth) combined with the influence of lower mobility.

Figure 7b shows the results of the same exercise, but applied to the latest forecast. The results are similar, again indicating that accumulated natural immunity is the dominant factor behind the steep forecast decline in infections over at least the next 30 days. Cold winter weather also remains a factor restraining even steeper declines. Mobility, however, plays very little role in the latest forecast, suggesting that mobility, which increased after the early January infections peak, is now neither contributing to nor restraining the forecasted decline ahead.

In sum, these results suggest the dominate driver of the steep forecasted decline in COVID-19 infections from the early January 2021 peak through mid-February (the time of this writing), as well as the forecasted continued decline into April is accumulated natural immunity and not improved social distancing behavior, beneficial weather, or vaccinations. Going forward, continued vaccinations and warmer temperatures would be expected to steepen the decline, while increases in mobility would slow the decline.

There are two important risks to the forecast that should be noted. First, the model assumes no possiblity of reinfection. It is not known how long COVID-19 immunity – either due to prior infections or to vaccinations – lasts. In addition, it is possible that recent and future new variants of the virus could be capable of reinfecting previously infected individuals. Future versions of the model could potentially account for reinfections by applying a depreciation rate to the term measuring accumulated natural immunity.

Second, new variants could increase the transmissibility of the virus, implying a larger elasticity of mobility on infection growth than what was estimated using the data to date. One way to assess whether this elasticity has increased is through rolling regressions, which I report in Figure A4. Specifically, I re-estimate the mobility IRFs presented in panel (a) of Figures 2 repeatedly using rolling samples. That is, I estimate the IRFs first using data on

the independent variables for the 140 day (14-period) sample ending with Sept. 16, 2020, then using the 140 day sample ending Sept. 26, and so on until the latest 10-day period of available data, which ended Jan. 24. The dependent variables use data for a given horizon, which I specify as 30 days (3 periods), beyond the "ending" period for each rolling sample. Thus, the final subsample uses data on new infections through Feb. 19. To summarize how the results changed over time, I plot the 30-days-ahead mobility IRF coefficient (and its confidence interval) against the sample end-date. Though the mobility elasticity has increased somewhat for a couple of the mobility measures, in general the elasticity estimates have been stable over time to date.

6 Conclusion

This paper developed a semi-structural, econometric model useful for understanding and forecasting infectious disease spread and applied it to forecasting COVID-19 infections at the county and national level. The model is derived from the standard SIR epidemiological model and it relates subsequent growth in active infections to cumulative infections to date as well as current and lagged values of transmission factors such as mobility and weather. The model is estimated using near real-time, county-level data on mobility, weather, and COVID-19 cases. Predicted values from the estimated model provided provisional out-of-sample forecasts of COVID-19 infections by county at horizons ranging from 10 days ahead to 70 days ahead. Final forecasts were obtained by augmenting the provisional forecasts to account for vaccinations to date. Prior forecasts were found to be fairly accurate, especially in terms of the geographical/cross-sectional distribution of COVID-19 infections and in terms of the national aggregate forecast.

The latest forecasts, using data through February 19, 2021, predict steep declines in infections in most parts of the country over the next several weeks. Nationally, infections were predicted to fall by 59% over the subsequent 30 days. Decomposing the drivers of the latest forecast, I found that accumulated natural immunity (i.e., cumulative infections to date, a.k.a. "seroprevalence") – not social distancing or vaccinations (yet) – is the primary factor exerting a strong downward pull on new infections. This finding has an important implication: Because accumulated natural immunity should only increase in the near-term, the decline in cases is unlikely to reverse in the near-term. Over the longer term, infections could rise again if either immunity stemming from earlier infections or vaccinations begins to wane or new variants emerge that are resistant to vaccinations and/or increase the transmissibility associated with mobility.

References

Atkinson, T., Dolmas, J., Koch, C., Koenig, E. F., Mertens, K., Murphy, A. & Yi, K.-M. (2020), 'Mobility and engagement following the sars-cov-2 outbreak', *FRB of Dallas Working Paper* (2014).

Badr, H., Du, H., Marshall, M., Dong, E., Squire, M. & Gardner, L. M. (2020), 'Social distancing is effective at mitigating covid-19 transmission in the united states', *medRxiv* .

Barro, R. J. (2020), Non-pharmaceutical interventions and mortality in us cities during the great influenza pandemic, 1918-1919, Technical report, National Bureau of Economic Research.

Barro, R. J., Ursúa, J. F. & Weng, J. (2020), The coronavirus and the great influenza pandemic: Lessons from the "spanish flu" for the coronavirus's potential effects on mortality and economic activity, Technical report, National Bureau of Economic Research.

Bisin, A. & Moro, A. (2020), Learning epidemiology by doing: The empirical implications of a spatial-sir model with behavioral responses, Technical report, National Bureau of Economic Research.

Carleton, T., Cornetet, J., Huybers, P., Meng, K. & Proctor, J. (2020), 'Ultraviolet radiation decreases covid-19 growth rates: Global causal estimates and seasonal implications', *Available at SSRN 3588601* .

Carson, R. T., Carson, S. L., Dye, T. K., Mayfield, S. L., Moyer, D. C. & Chu, A. Y. (2020), 'Covid-19's us temperature response profile', *medRxiv* .

Chen, L. & Spence, M. (2020), 'Five lessons from tracking the global pandemic economy', *VoxEU* .

Desmet, K. & Wacziarg, R. (2020), 'Understanding spatial variation in covid-19 across the united states'.

Fernández-Villaverde, J. & Jones, C. I. (2020), Estimating and simulating a sird model of covid-19 for many countries, states, and cities, Technical report, National Bureau of Economic Research.

Flaxman, S., Mishra, S., Gandy, A., Unwin, H. J. T., Mellan, T. A., Coupland, H., Whittaker, C., Zhu, H., Berah, T., Eaton, J. W. et al. (2020), 'Estimating the effects of non-pharmaceutical interventions on covid-19 in europe', *Nature* pp. 1–5.

Glaeser, E. L., Gorback, C. S. & Redding, S. J. (2020), How much does covid-19 increase with mobility? evidence from new york and four other us cities, Technical Report 27519, National Bureau of Economic Research.

Goodman-Bacon, A. & Marcus, J. (2020), Using difference-in-differences to identify causal effects of covid-19 policies, Technical report, DIW Berlin Discussion Paper.

Hsiang, S., Allen, D., Annan-Phan, S., Bell, K., Bolliger, I., Chong, T., Druckenmiller, H., Huang, L. Y., Hultgren, A., Krasovich, E. et al. (2020), 'The effect of large-scale anti-contagion policies on the covid-19 pandemic', *Nature* pp. 1–9.

Jamil, T., Alam, I., Gojobori, T. & Duarte, C. M. (2020), 'No evidence for temperature-dependence of the covid-19 epidemic', *MedRxiv* .

Jordà, Ò. (2005), 'Estimation and inference of impulse responses by local projections', *American economic review* **95**(1), 161–182.

Kapoor, R., Rho, H., Sangha, K., Sharma, B., Shenoy, A. & Xu, G. (2020), 'God is in the rain: The impact of rainfall-induced early social distancing on covid-19 outbreaks', *Available at SSRN 3605549* .

Lemaitre, J. C., Grantz, K. H., Kaminsky, J., Meredith, H. R., Truelove, S. A., Lauer, S. A., Keegan, L. T., Shah, S., Wills, J., Kaminsky, K., Perez-Saez, J., Lessler, J. & Lee, E. C. (2020), 'A scenario modeling pipeline for covid-19 emergency planning', *medRxiv* .
URL: *https://www.medrxiv.org/content/early/2020/09/11/2020.06.11.20127894*

Liu, L., Moon, H. R. & Schorfheide, F. (2021), 'Panel forecasts of country-level covid-19 infections', *Journal of Econometrics* **220**(1), 2 – 22. Themed Issue: Pandemic Econometrics / Covid Pandemics.
URL: *http://www.sciencedirect.com/science/article/pii/S030440762030347X*

Soucy, J.-P. R., Sturrock, S. L., Berry, I., Westwood, D. J., Daneman, N., MacFadden, D. R. & Brown, K. A. (2020), 'Estimating effects of physical distancing on the covid-19 pandemic using an urban mobility index', *medRxiv* .
URL: *https://www.medrxiv.org/content/early/2020/05/24/2020.04.05.20054288*

Unwin, H. J. T., Mishra, S., Bradley, V. C., Gandy, A., Mellan, T. A., Coupland, H., Ish-Horowicz, J., Vollmer, M. A., Whittaker, C., Filippi, S. L. et al. (2020), 'State-level tracking of covid-19 in the united states', *Nature communications* **11**(1), 1–9.

Wilson, D. J. (2019), 'Clearing the fog: The predictive power of weather for employment reports and their asset price responses', *American Economic Review: Insights* **1**(3), 373–88.

Xu, R., Rahmandad, H., Gupta, M., DiGennaro, C., Ghaffarzadegan, N., Amini, H. & Jalali, M. S. (2020), 'The modest impact of weather and air pollution on covid-19 transmission', *medRxiv* .

Table 1

Dynamic Impacts of Mobility and Weather on COVID-19 Transmission 30 Days Ahead

Dependent Variable is $log(I_{t+3}) - log(I_t)$. Various Mobility Measures (columns)

	(1) MEI	(2) Work	(3) Transit	(4) Retail & Rest.	(5) Grocery & Pharmacy	(6) Parks
dlog(I)	-0.261***	-0.239***	-0.129***	-0.178***	-0.148***	-0.0613
	(0.0217)	(0.0220)	(0.0309)	(0.0261)	(0.0299)	(0.0411)
Mobility	0.582***	1.970***	0.336***	0.869***	0.684***	0.0632
	(0.211)	(0.439)	(0.115)	(0.241)	(0.179)	(0.113)
L.Mobility	0.368	1.425***	0.152	0.523*	0.455*	0.327***
	(0.220)	(0.383)	(0.162)	(0.275)	(0.233)	(0.115)
L2.Mobility	0.0941	-0.177	-0.0454	0.154	-0.00973	0.173**
	(0.103)	(0.387)	(0.163)	(0.187)	(0.178)	(0.0764)
L3.Mobility	-0.0737	-0.605	0.0588	-0.362	-0.127	-0.100
	(0.0681)	(0.486)	(0.140)	(0.222)	(0.302)	(0.106)
logmaxtemp	-0.465	-0.517	-0.819**	-0.752**	-0.763*	-1.027***
	(0.314)	(0.330)	(0.386)	(0.354)	(0.377)	(0.333)
L.logmaxtemp	0.214	0.187	0.171	0.0398	0.0790	-0.158
	(0.447)	(0.449)	(0.427)	(0.422)	(0.429)	(0.320)
L2.logmaxtemp	0.583	0.668	0.858*	0.645	0.809	0.808*
	(0.521)	(0.543)	(0.487)	(0.525)	(0.557)	(0.437)
L3.logmaxtemp	1.075**	1.012**	1.160**	1.177**	1.312**	1.344***
	(0.458)	(0.469)	(0.460)	(0.467)	(0.497)	(0.444)
Precipitation	-0.000939	0.00124	0.00414	0.00243	0.00170	0.00614
	(0.00439)	(0.00503)	(0.00514)	(0.00520)	(0.00541)	(0.00529)
L.Precipitation	-0.00374	-0.00191	0.00150	-0.00306	-0.00251	-0.00000548
	(0.00425)	(0.00425)	(0.00426)	(0.00393)	(0.00392)	(0.00465)
L2.Precipitation	-0.000897	-0.00140	0.000669	-0.00259	-0.00240	-0.000737
	(0.00494)	(0.00584)	(0.00648)	(0.00558)	(0.00581)	(0.00559)
L3.Precipitation	0.00106	0.00266	0.00442	-0.000772	0.000608	0.000496
	(0.00542)	(0.00601)	(0.00633)	(0.00580)	(0.00603)	(0.00578)
3*log(1 - cases p.c.)	8.474***	7.806***	7.403***	7.973***	8.151***	7.416***
	(0.965)	(0.934)	(0.877)	(0.953)	(1.023)	(0.967)
Constant	-4.672**	-4.142**	-5.000**	-3.746*	-5.275**	-3.498*
	(1.775)	(1.892)	(1.984)	(1.996)	(2.007)	(1.923)
Observations	64337	55560	21879	36804	33125	14925
Adjusted R^2	0.386	0.411	0.441	0.451	0.454	0.504
Dep. Variable Mean						
Mobility Mean						

* $p < 0.10$, ** $p < 0.05$, *** $p < 0.01$

Table 2: Forecast Accuracy Statistics

Horizon (Days)	(1) Correlation	(2) RMSFE	(3) Mean Actual Value	(4) Mean Predicted Value	(5) No.
10	0.4608	0.2610	-0.3781	-0.3672	2651
20	0.4369	0.3861	-0.6689	-0.6894	2653
30	0.4361	0.4488	-0.9781	-0.9932	2653
40	0.4800	0.5195	-1.1179	-1.0169	2682
50	0.5017	0.6128	-0.8865	-0.6981	2746
60	0.5655	0.8946	-1.0183	-0.4416	2750
70	0.6795	1.0085	-0.9593	-0.2654	2755

Note: The values shown in columns (2) to (4) are based on population-weighted means.

Figure 1: Mobility Over Time

(a) Mobility & Engagement Index (MEI)

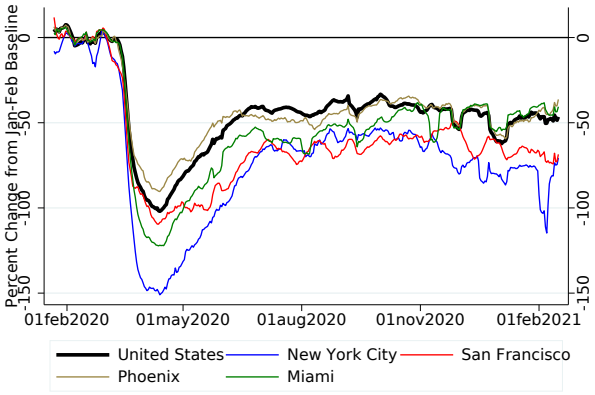

(b) Visits to Workplaces

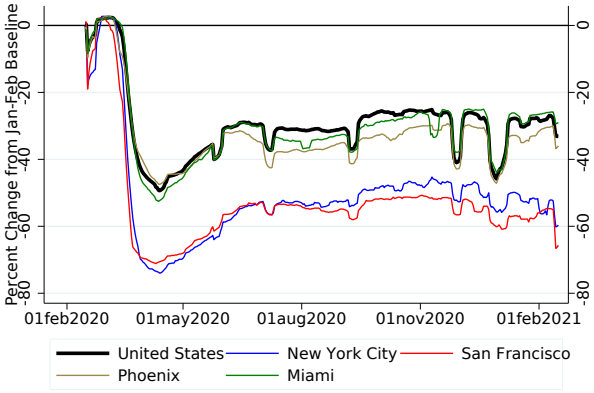

Figure 2: Dynamic Impacts of Mobility on COVID-19 Transmission

Impulse Response Functions Estimated by Panel Linear Projections

(a) Mobility & Engagement Index

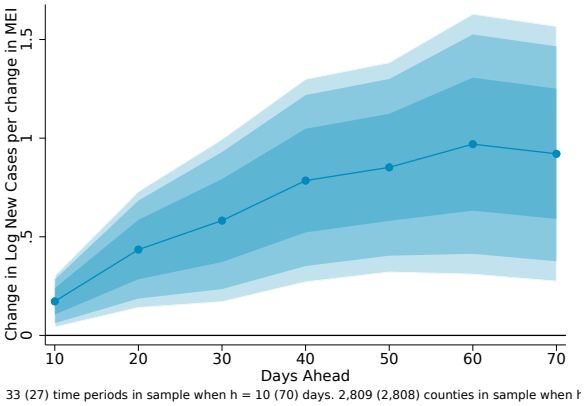

(b) Visits to Workplaces

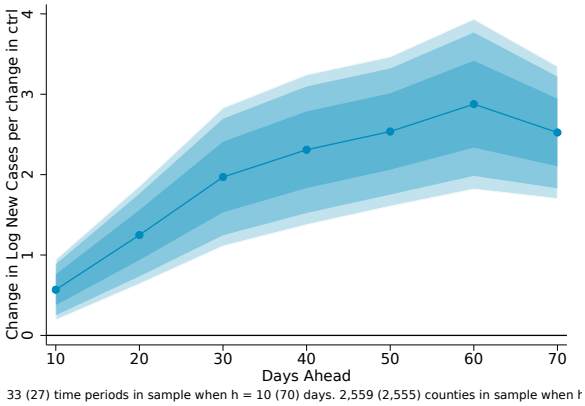

(c) Visits to Transit Stations

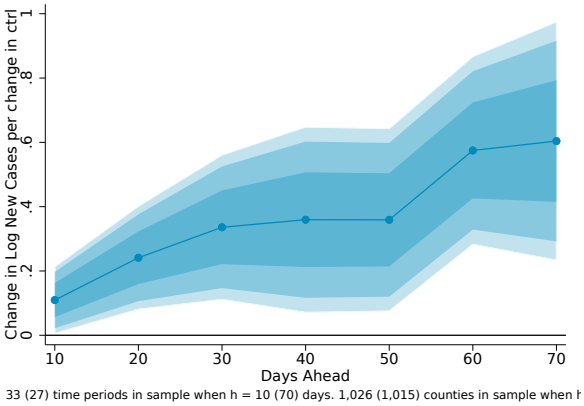

(d) Visits to Retail and Restaurants

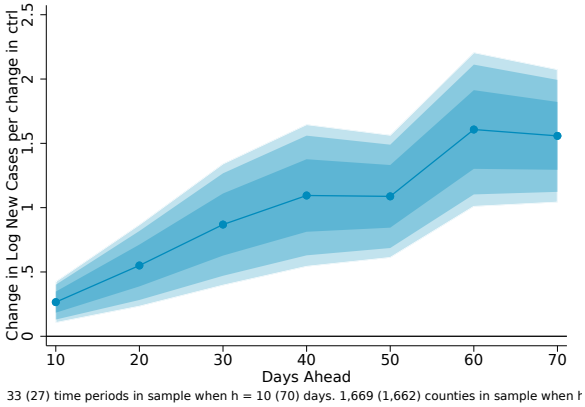

(e) Visits to Grocery and Pharmacy

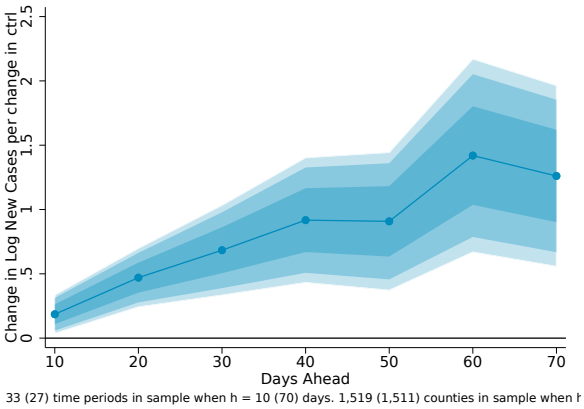

(f) Visits to Parks

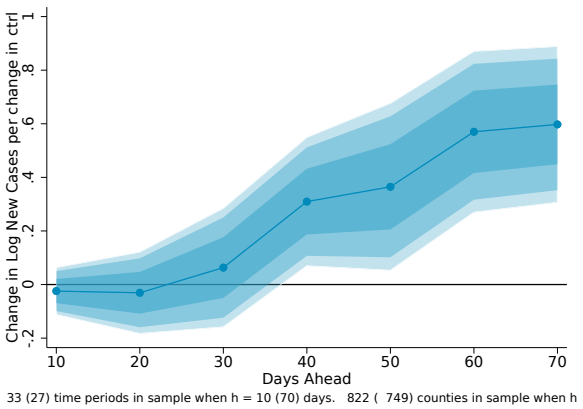

Note: Estimates of equation 9 in the text using panel local projections regressions. Shaded regions are 68 (one standard error), 90, and 95 percent confidence intervals (from darkest to lightest).

Figure 3: Dynamic Impacts of Weather on COVID-19 Cases

Impulse Response Functions Estimated by Panel Linear Projections

(a) Log Daily Max Temperature

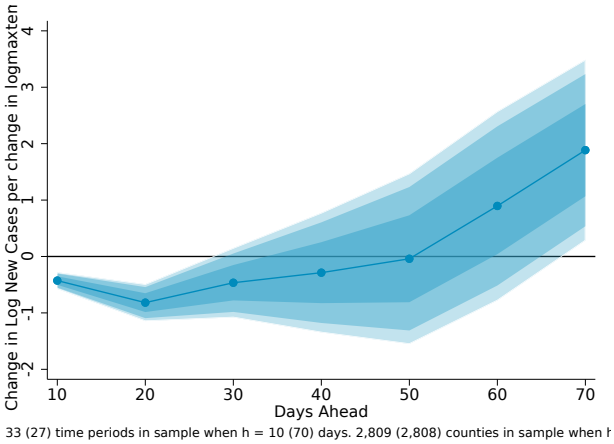

(b) Precipitation

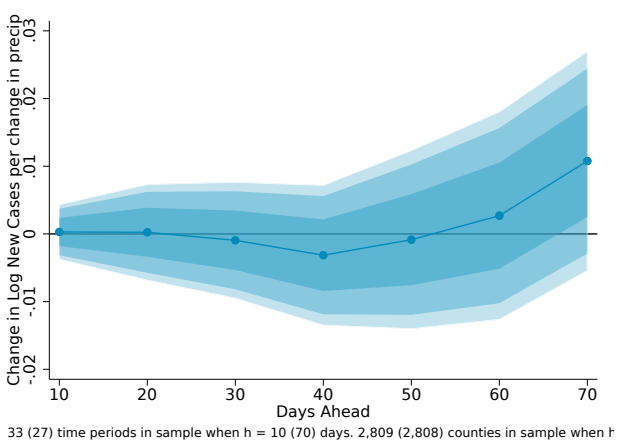

Note: Estimates of equation 9 in the text using panel local projections regressions. Shaded regions are 68 (one standard error), 90, and 95 percent confidence intervals (from darkest to lightest).

Figure 4: Projected Growth of COVID-19 Infections By County, 30 Days Ahead

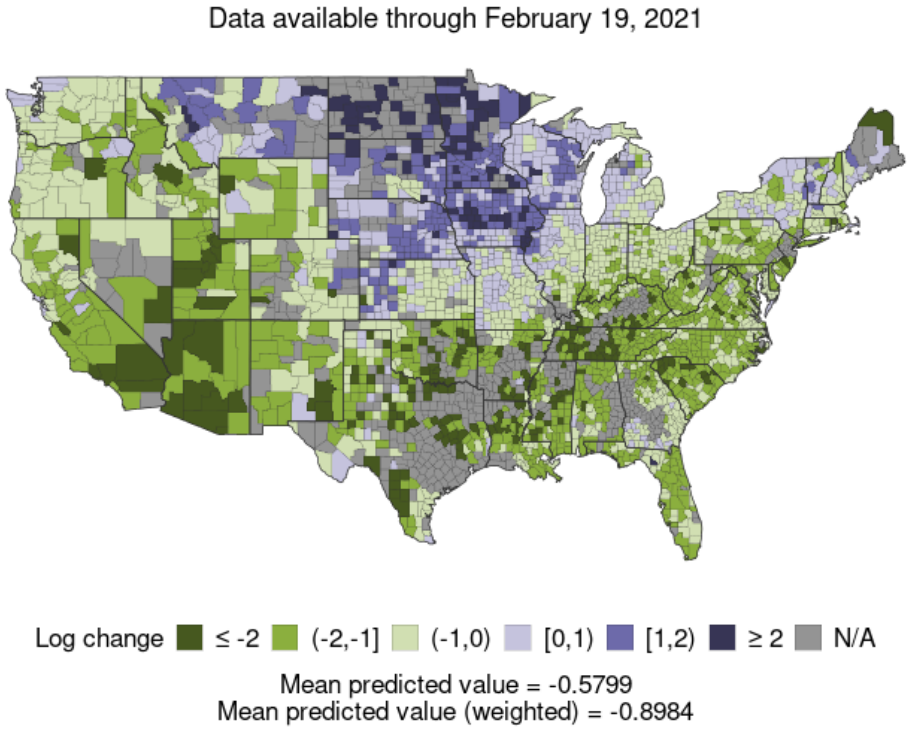

Note: Map 1 shows each county's projected growth in infections, color-coded into one of five groups, ranked from the most negative to most positive; gray shading indicates insufficient data. Growth is measured by the change in log active infections from the date listed to 30 days later.

Figure 5: Historical and Projected Active COVID-19 Infections in the U.S.

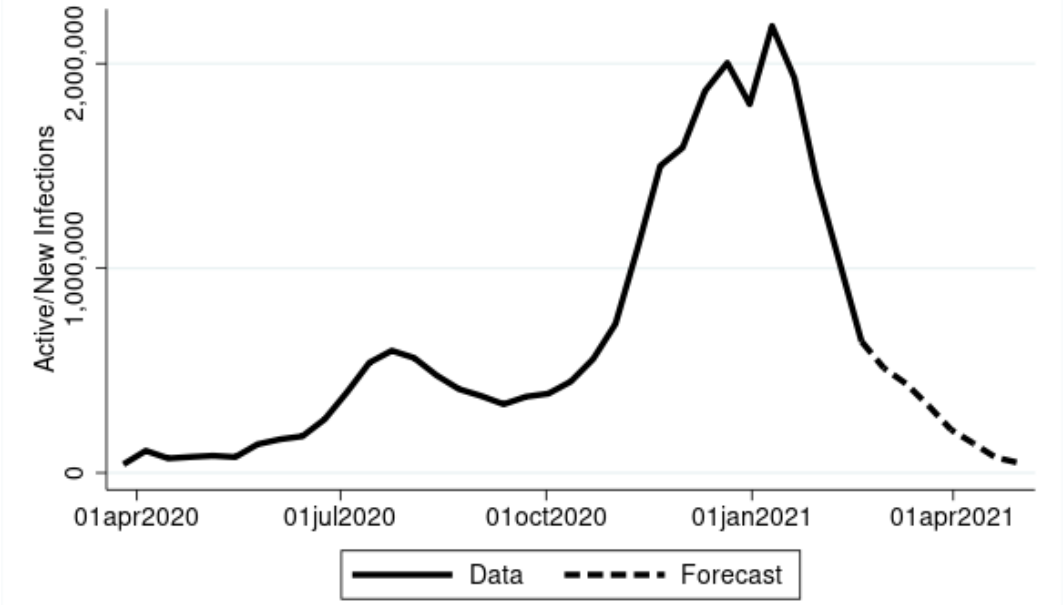

Figure 6: Previous Forecasts

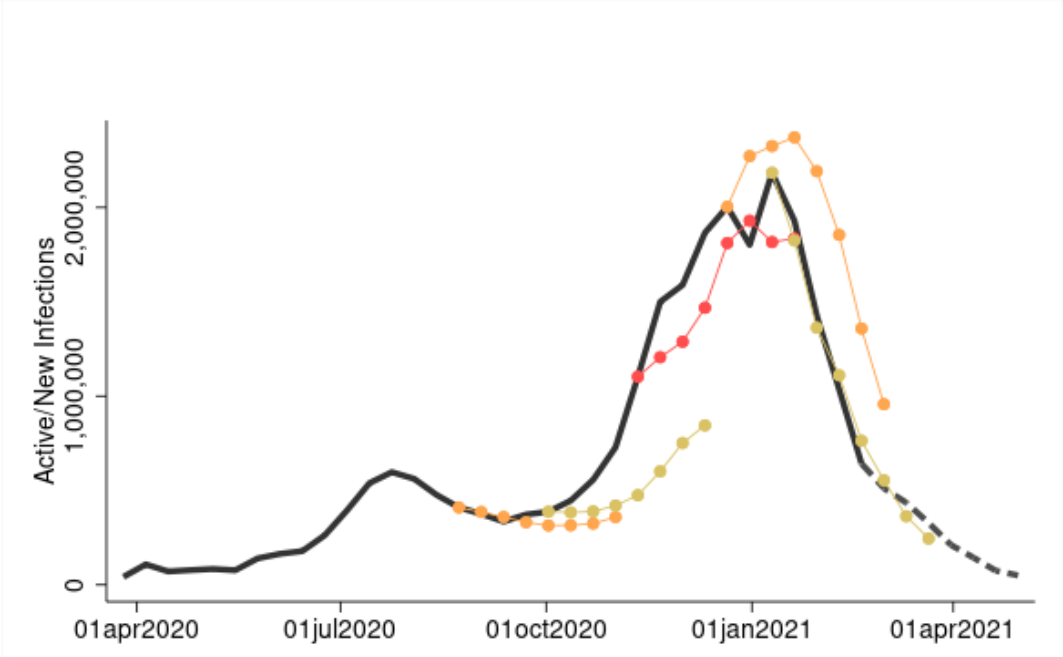

Note: The solid black line plots actual data on active/new COVID-19 infections to date. The dashed blue line plots the out-of-sample forecast based on the latest available data. The other series show previous forecasts based on data (and estimated model) available at the start of each forecast period (indicated by the first dot of the plotted series).

Figure 7: Key Factors Driving the Forecast

(a) Forecast on January 10, 2021

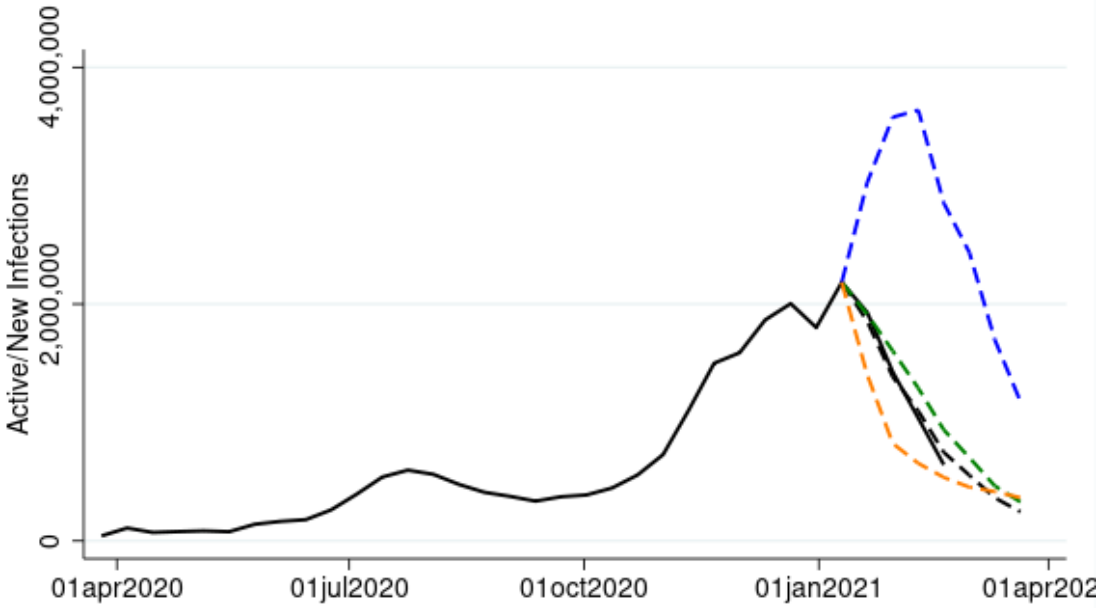

(b) Latest Forecast

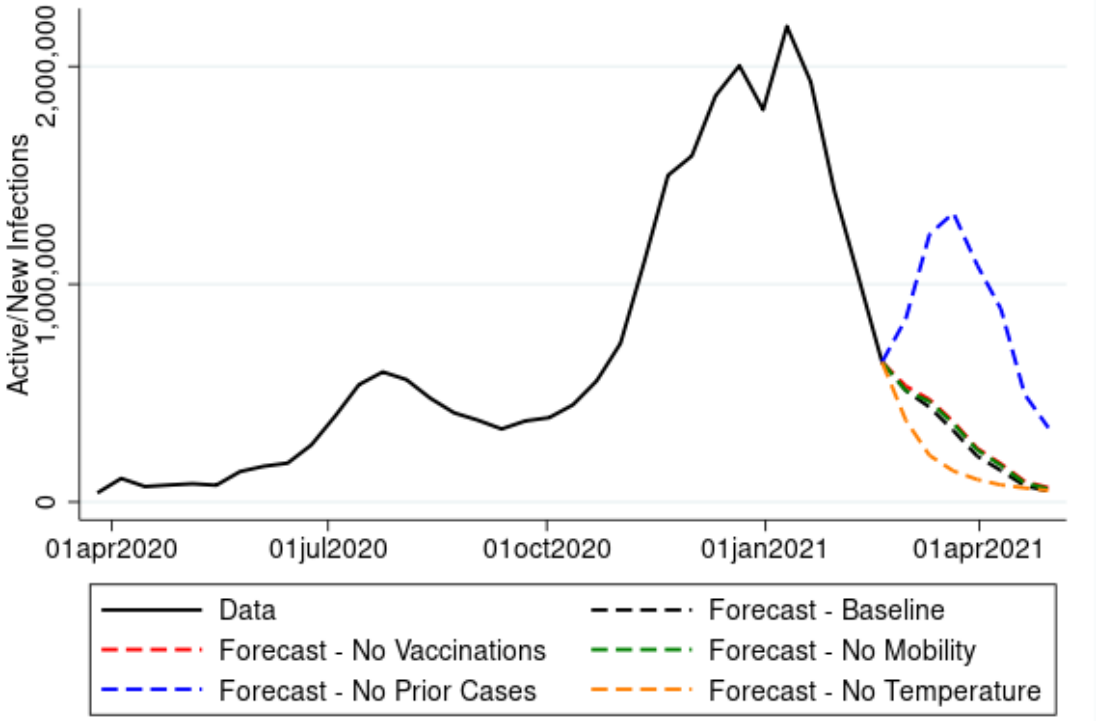

Note: The solid black line plots actual data on active/new COVID-19 infections to date. The dashed blue line plots the out-of-sample forecast based on data through 1/20/21 (top figure) or latest available (top figure). The other series show forecasts with various components of the model "turned off" (i.e., set equal to their predicted values based on county mean).

ONLINE APPENDIX

Table A1

Dynamic Impacts of Mobility and Weather on COVID-19 Transmission 30 Days Ahead

Dependent Variable is $log(I_{t+3}) - log(I_t)$. Various Mobility Measures (columns)

No Time Fixed Effects

	(1) MEI	(2) Work	(3) Transit	(4) Retail & Rest.	(5) Grocery & Pharmacy	(6) Parks
dlog(I)	-0.197***	-0.192***	0.0255	-0.0598	0.0220	0.136*
	(0.0187)	(0.0190)	(0.0452)	(0.0374)	(0.0459)	(0.0689)
Mobility	0.514**	1.991***	0.427*	1.061***	1.043*	0.147
	(0.209)	(0.356)	(0.248)	(0.354)	(0.555)	(0.182)
L.Mobility	0.446*	1.788***	0.789**	0.860**	0.906	0.535**
	(0.221)	(0.308)	(0.315)	(0.354)	(0.568)	(0.218)
L2.Mobility	0.319**	1.815***	0.301	0.609**	0.428	0.266
	(0.125)	(0.238)	(0.264)	(0.272)	(0.605)	(0.220)
L3.Mobility	-0.0643	-0.680**	-0.568*	-0.430	-1.120	-0.314
	(0.110)	(0.311)	(0.282)	(0.385)	(0.722)	(0.225)
logmaxtemp	-1.262***	-0.820***	-1.791***	-1.723***	-1.742***	-2.016***
	(0.270)	(0.267)	(0.342)	(0.316)	(0.380)	(0.343)
L.logmaxtemp	-0.473	-0.411	-0.392	-0.489	-0.382	-0.773*
	(0.293)	(0.444)	(0.426)	(0.342)	(0.461)	(0.442)
L2.logmaxtemp	0.0335	0.242	0.617	0.398	0.733	0.711
	(0.368)	(0.507)	(0.393)	(0.352)	(0.455)	(0.472)
L3.logmaxtemp	0.807**	0.291	1.375***	1.075**	1.498***	1.722***
	(0.386)	(0.398)	(0.473)	(0.439)	(0.539)	(0.484)
Precipitation	-0.0109	-0.00366	-0.00738	-0.00952	-0.0107	-0.00280
	(0.00757)	(0.00653)	(0.00974)	(0.00913)	(0.00982)	(0.00880)
L.Precipitation	-0.00921	-0.00217	-0.00431	-0.0107	-0.00839	-0.00333
	(0.00771)	(0.00649)	(0.0103)	(0.00928)	(0.0103)	(0.0102)
L2.Precipitation	-0.00793	-0.00523	-0.000383	-0.00589	-0.00169	-0.00159
	(0.00822)	(0.00817)	(0.0121)	(0.0101)	(0.0114)	(0.0122)
L3.Precipitation	-0.00255	0.000226	0.00662	-0.000740	0.00283	0.00255
	(0.00829)	(0.00769)	(0.0110)	(0.00951)	(0.0101)	(0.0102)
3*log(1 - cases p.c.)	8.619***	6.737***	5.637***	7.247***	5.664***	5.454***
	(0.947)	(0.757)	(0.784)	(0.739)	(0.827)	(0.829)
Constant	5.268***	5.145***	1.548	4.152**	0.153	1.869
	(1.767)	(1.507)	(1.712)	(1.556)	(1.658)	(1.547)
Observations	64337	55560	21879	36804	33125	14925
Adjusted R^2	0.272	0.320	0.225	0.271	0.231	0.252
Dep. Variable Mean						
Mobility Mean						

* $p < 0.10$, ** $p < 0.05$, *** $p < 0.01$

Figure A1: Dynamic Impacts of Mobility on COVID-19 Transmission

Results Based on Deaths Data Instead of Cases Data

(a) Mobility & Engagement Index (MEI)

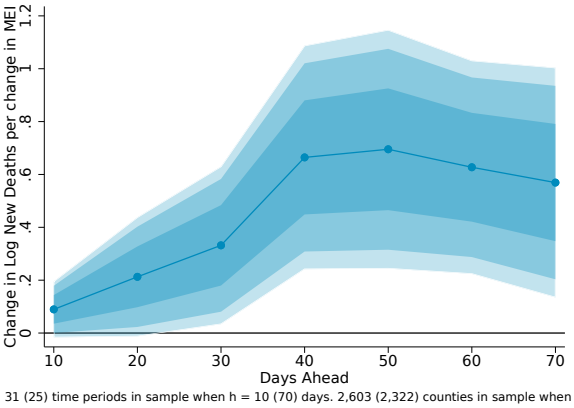

31 (25) time periods in sample when h = 10 (70) days. 2,603 (2,322) counties in sample when h

(b) Visits to Workplaces

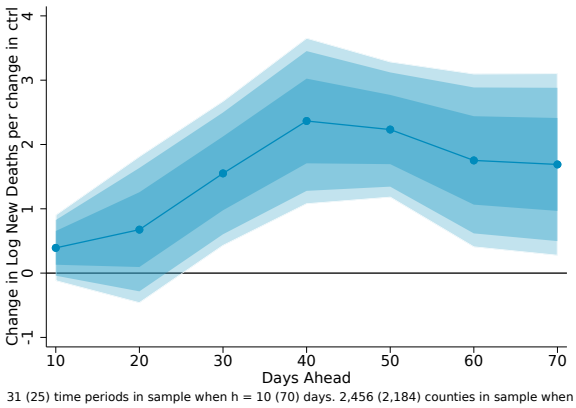

31 (25) time periods in sample when h = 10 (70) days. 2,456 (2,184) counties in sample when h

(c) Visits to Transit Stations

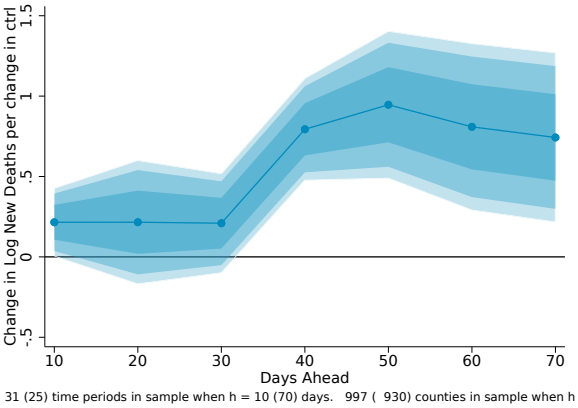

31 (25) time periods in sample when h = 10 (70) days. 997 (930) counties in sample when h

(d) Visits to Retail and Restaurants

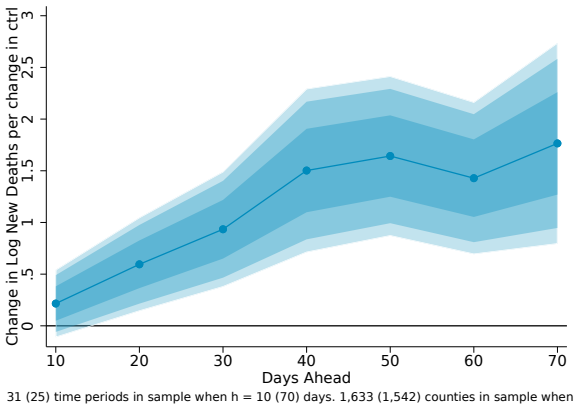

31 (25) time periods in sample when h = 10 (70) days. 1,633 (1,542) counties in sample when h

(e) Visits to Grocery and Pharmacy

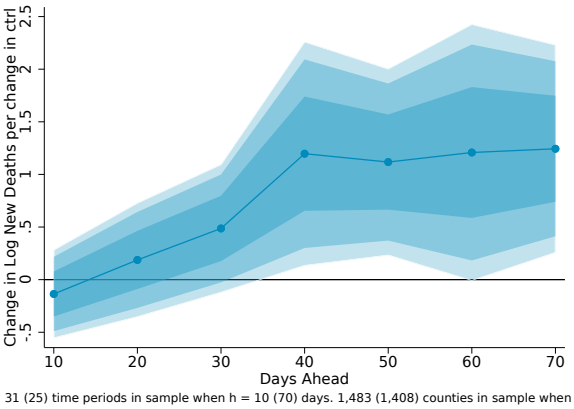

31 (25) time periods in sample when h = 10 (70) days. 1,483 (1,408) counties in sample when h

(f) Visits to Parks

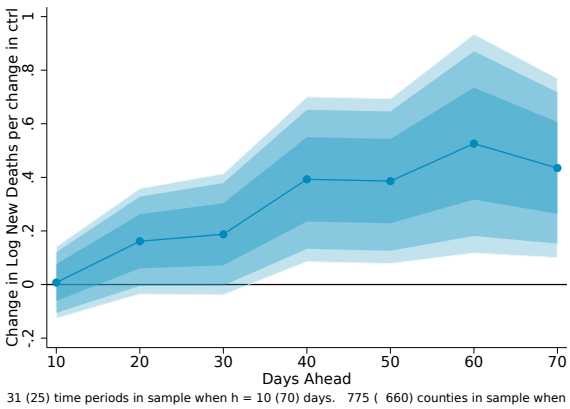

31 (25) time periods in sample when h = 10 (70) days. 775 (660) counties in sample when h

Note: Estimates of equation 9 in the text using panel local projections regressions. Shaded regions are 68 (one standard error), 90, and 95 percent confidence intervals (from darkest to lightest).

Figure A2: Dynamic Impacts of Mobility on Subsequent Mobility

Impulse Response Functions Estimated by Panel Linear Projections

(a) Mobility & Engagement Index

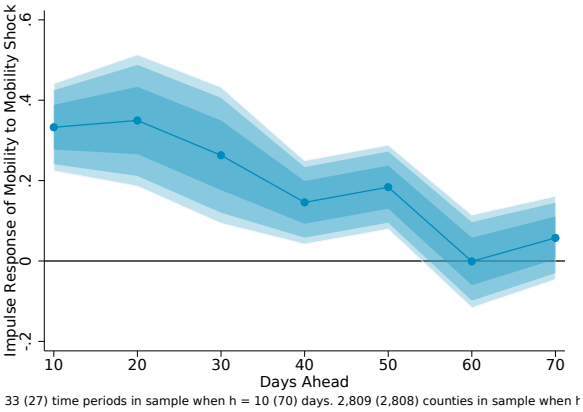

(b) Visits to Workplaces

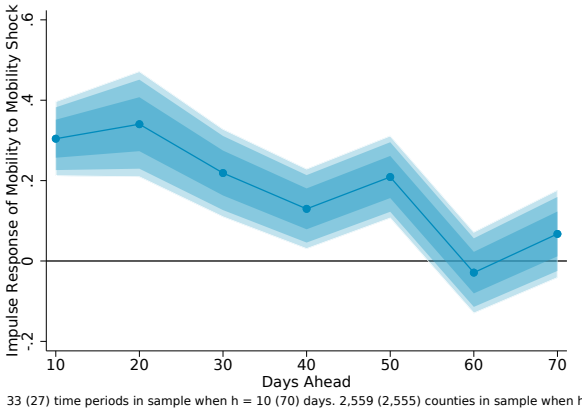

(c) Visits to Transit Stations

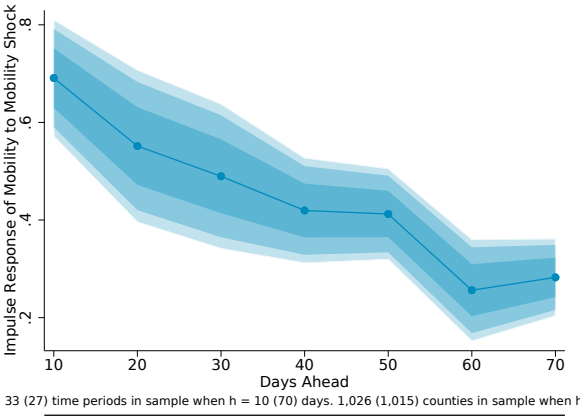

(d) Visits to Retail and Restaurants

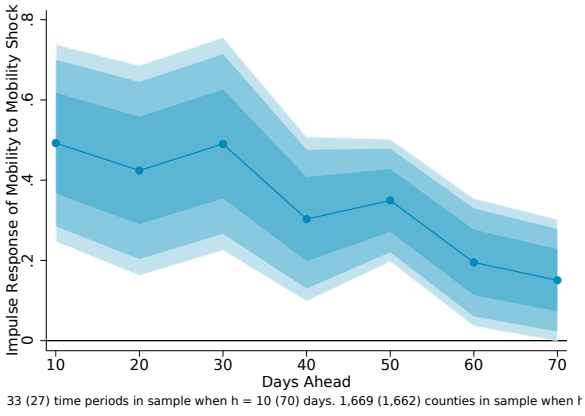

(e) Visits to Grocery and Pharmacy

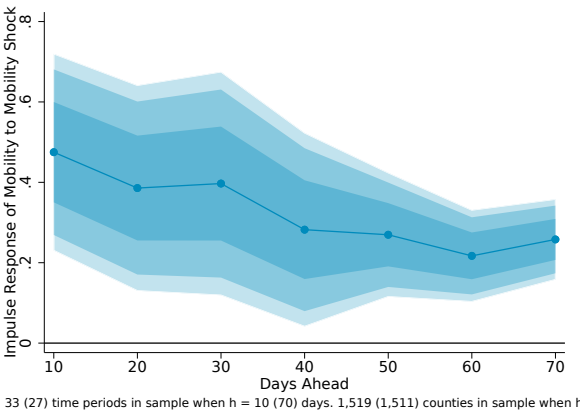

(f) Visits to Parks

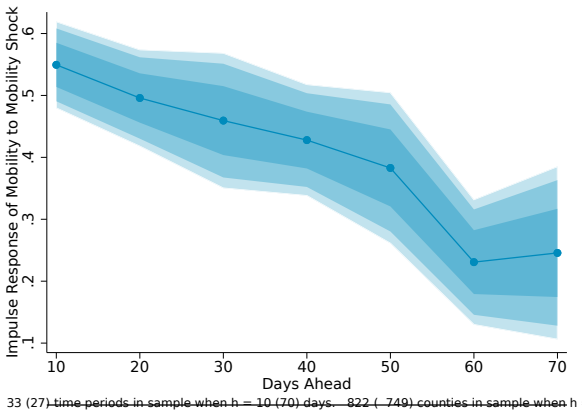

Note: Estimates of equation 9 in the text using panel local projections regressions. Shaded regions are 68 (one standard error), 90, and 95 percent confidence intervals (from darkest to lightest).

Figure A3: Dynamic Impacts of Mobility on COVID-19 Transmission

No Time Fixed Effects (Only County Fixed Effects)

(a) Mobility & Engagement Index (MEI)

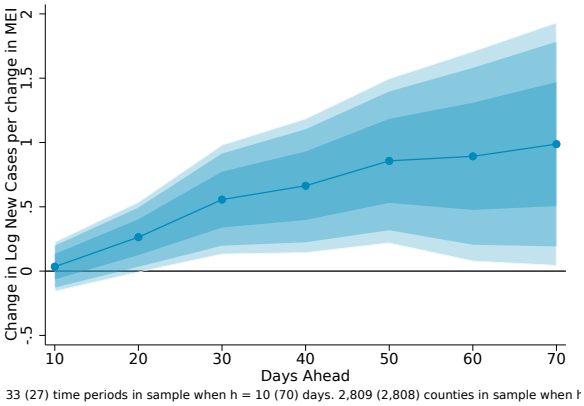

(b) Visits to Workplaces

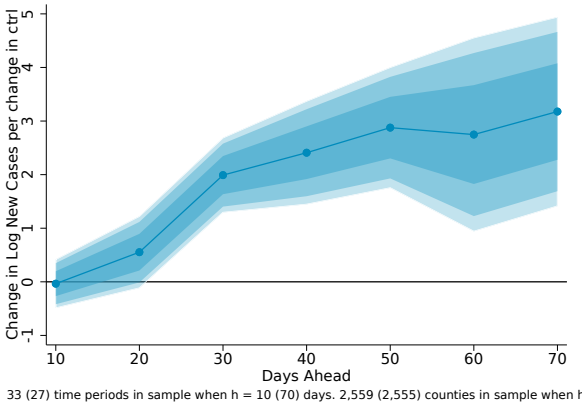

(c) Visits to Transit Stations

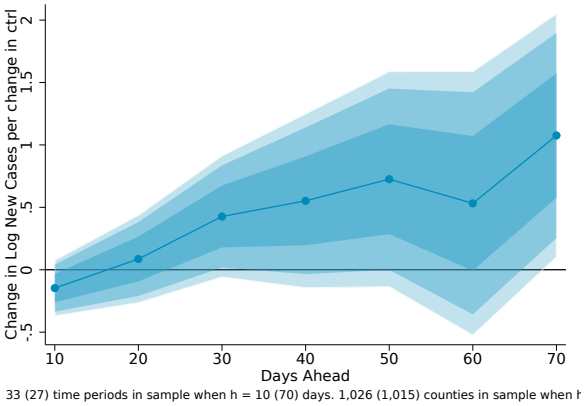

(d) Visits to Retail and Restaurants

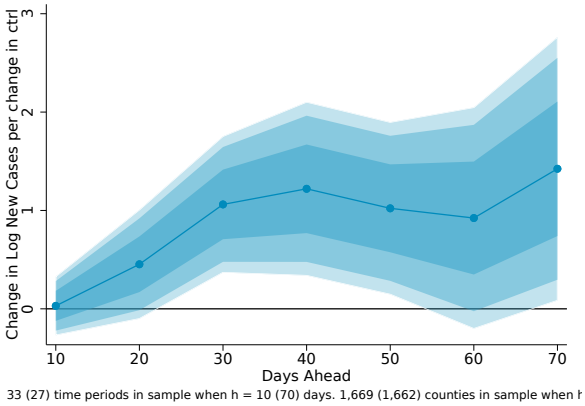

(e) Visits to Grocery and Pharmacy

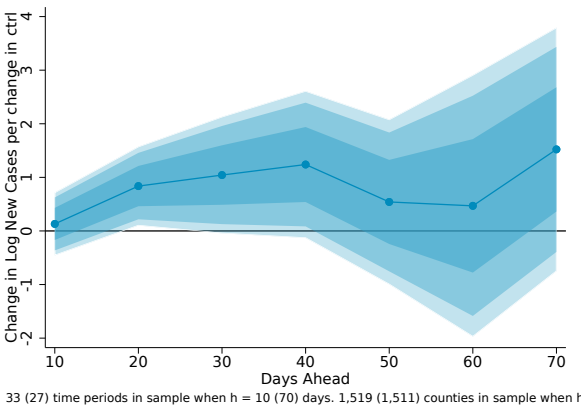

(f) Visits to Parks

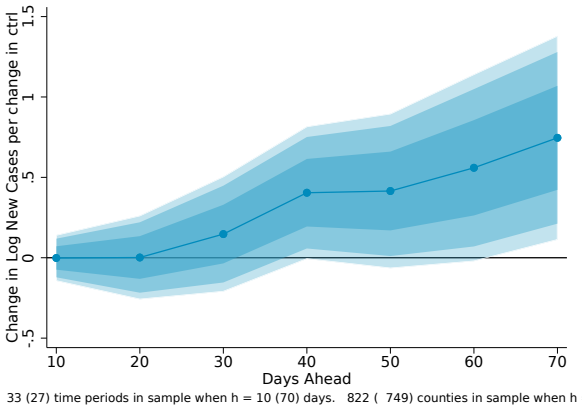

Note: Estimates of equation 9 in the text using panel local projections regressions. Shaded regions are 68 (one standard error), 90, and 95 percent confidence intervals (from darkest to lightest).

Figure A4: Rolling Regressions (140-Day Windows)

Impact of Mobility on COVID-19 Cases Growth 30-Days Ahead

(a) Mobility & Engagement Index (MEI)

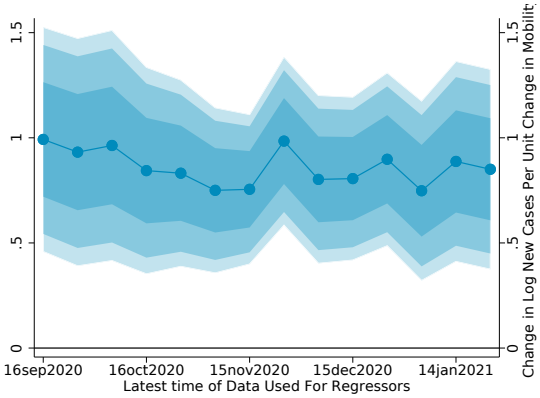

(b) Visits to Workplaces

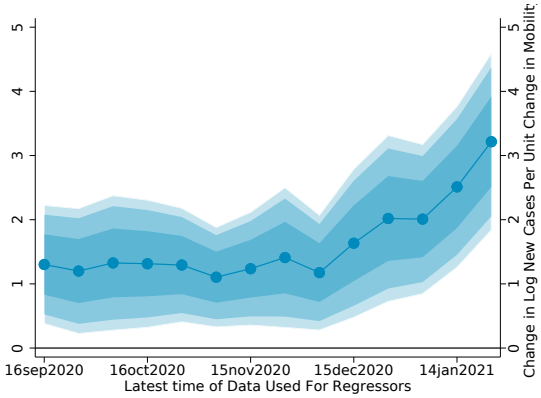

(c) Visits to Transit Stations

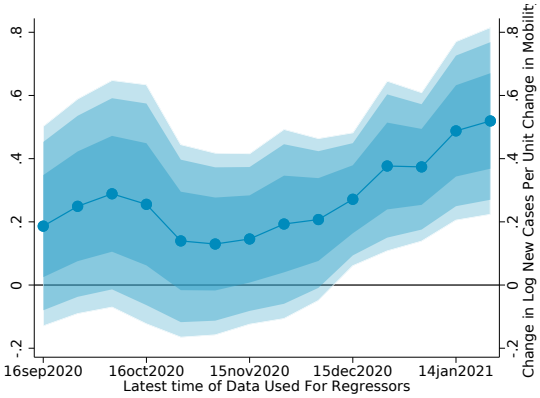

(d) Visits to Retail and Restaurants

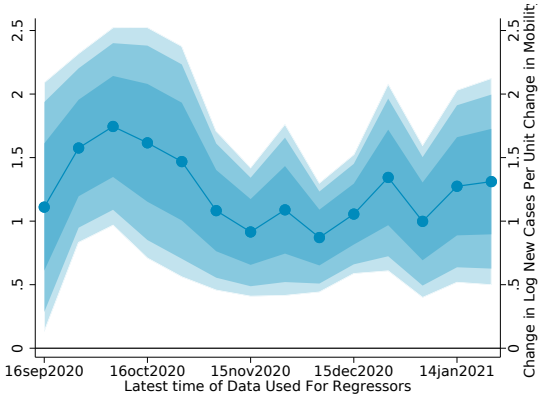

(e) Visits to Grocery and Pharmacy

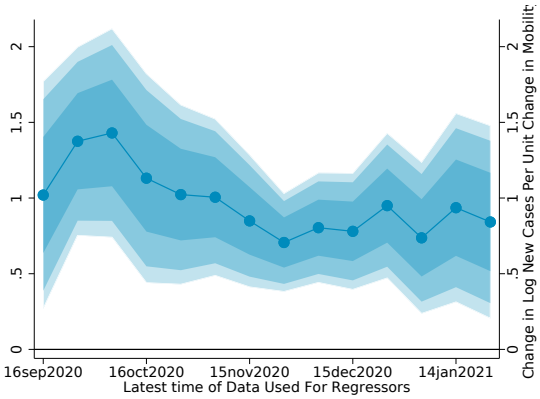

(f) Visits to Parks

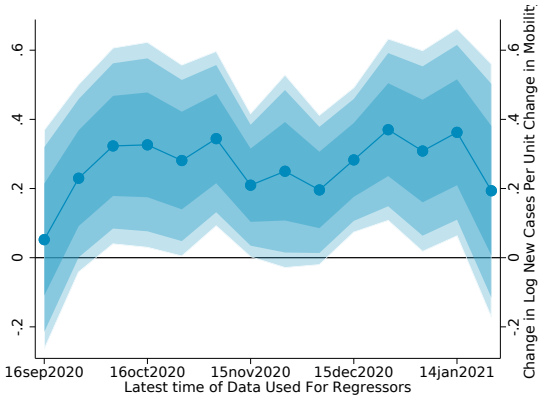

Note: Shaded regions are 68 (one standard error), 90, and 95 percent confidence intervals (from darkest to lightest).

Figure A5: Projected Growth of COVID-19 Infections By County

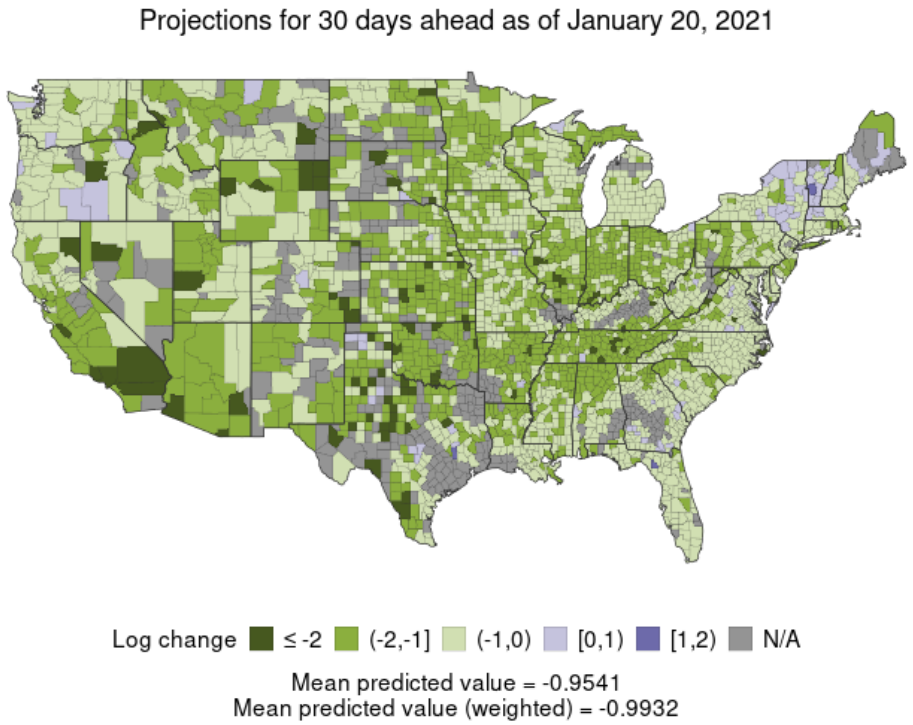

Figure A6: Actual Growth of COVID-19 Infections By County

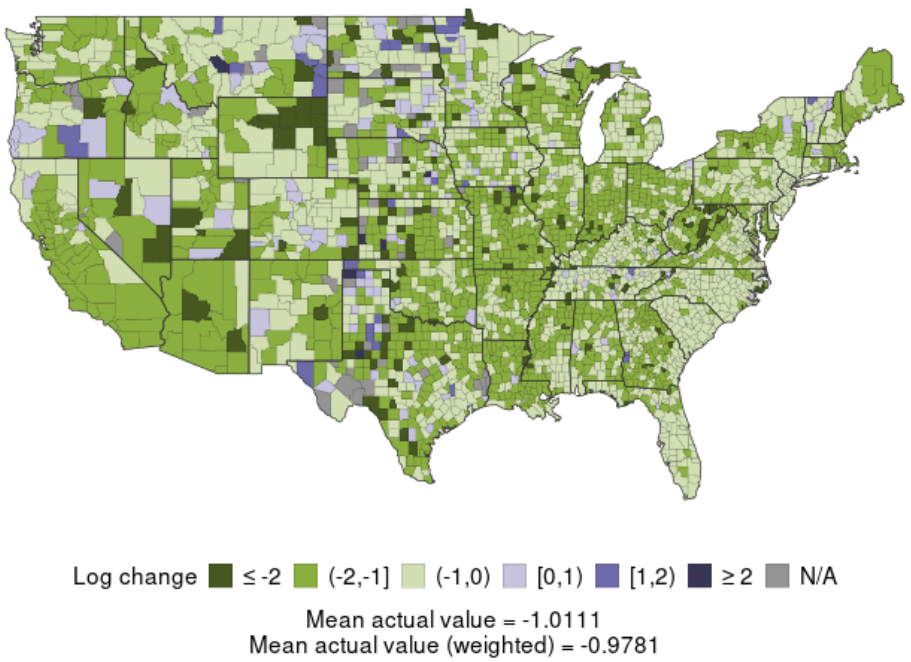

Note: Counties are color-coded based on the 30-day change in the log number of infectious persons.